

# Meteorology and Ozone, Temperature, Relative Humidity

J. Coates<sup>1</sup> and T. Butler<sup>1</sup>

<sup>1</sup>Institute for Advanced Sustainability Studies, Potsdam, Germany

December 23, 2015

## Abstract

## 1 Introduction

Surface-level ozone ( $O_3$ ) is a secondary air pollutant formed from the photochemical degradation of volatile organic compounds (VOCs) in the presence of nitrogen oxides ( $NO_x$ ). Due to the photochemical nature of ozone production, meteorological factors such as temperature strongly influence ozone production (Jacob and Winner, 2009). Temperature influences ozone production through temperature-dependent emissions of VOC from biogenic sources (anthropogenic emissions are typically not temperature dependent) and the reaction rates of many of the chemical reactions involved in producing ozone are also temperature dependent. The recent review of Pusede et al. (2015) provides a detailed description of the temperature-dependent processes impacting ozone production. A recent study by indicates that temperature is a major meteorological driver for ozone in central europe.

Many studies over the US (Sillman and Samson, 1995; Dawson et al., 2007; Pusede et al., 2014) have observed the relationship between ozone and temperature, noting that increased temperatures tend to lead to higher ozone levels, often exceeding local air quality guidelines. Some of these studies (Sillman and Samson, 1995; Dawson et al., 2007) include modelling experiments using regional chemical transport models which have indeed verified the observed increases in ozone with temperature. The increase in the thermal decomposition rate of PAN (peroxy acetyl nitrate) with temperature is commonly cited for the increase of ozone with temperature.

Noelia's  
paper

Environmental chamber studies have looked at the relationship of ozone with temperature using a particular mixture of VOCs. The chamber experiments of Carter et al. (1979) and Hatakeyama et al. (1991), also showed increases in ozone with temperature and have also linked this relationship to increased PAN decomposition at higher temperatures ( $T > 303$  K). Hatakeyama et al. (1991) looked primarily at the influence of  $\text{HO}_2\text{NO}_2$  decomposition on ozone production and induced that at lower temperatures ( $T < 303$  K)  $\text{HO}_2\text{NO}_2$  decomposition has a large influence on ozone production but the influence of PAN decomposition on ozone production increases with temperature.

Pusede et al. (2014) used observations over the San Joaquin Valley, California to infer a non-linear relationship of ozone production with temperature and  $\text{NO}_x$ , similar to the well-known non-linear relationship of ozone production on  $\text{NO}_x$  and VOC levels (Sillman, 1999). In fact, Pusede et al. (2014) show that temperature can be used as a surrogate for VOC levels when looking at the relationship of ozone across  $\text{NO}_x$  gradients. Moreover, the described relationship of ozone on both  $\text{NO}_x$  and temperature needs to be considered when looking at effective strategies to reduce levels of surface ozone.

Despite a wealth of studies looking at the effects of temperature on ozone chemistry, there have not been (to our knowledge) modelling studies focusing on these effects across different  $\text{NO}_x$  gradients and whether the observed relationships are well-represented by different chemical mechanisms used in air quality models. The review of Pusede et al. (2015) also highlights a lack of modelling studies looking at this non-linear relationship of ozone on temperature across  $\text{NO}_x$  gradients. In this study, we use an idealised box model to determine how ozone levels vary with temperature and across  $\text{NO}_x$  gradients. We separate the effects of temperature-dependent chemistry and VOC emissions on ozone production by performing simulations including a temperature-independent source of isoprene followed by simulations using a temperature-dependent source of isoprene.

The study of Rasmussen et al. (2013) looking at the change of ozone with temperature in California (termed the “Ozone-Climate Penalty”) indicates that changing the chemical mechanism used by a model may also change the Ozone-Climate Penalty and should be investigated. Finally, by repeating these simulations with different chemical mechanisms, we determine whether the temperature dependence of ozone production is reproduced across different  $\text{NO}_x$  gradients in these chemical mechanisms.

## 2 Methodology

### 2.1 Model Setup

- MECCA box model as described in Coates and Butler (2015) to broadly simulate the Benelux (Belgium, Netherlands and Luxembourg) region. As photolysis rates are parameterised by the solar zenith angle, the solar zenith angle of 51°N was used, representative of the central Benelux region.
- MECCA box model has been updated to include vertical mixing with the free troposphere and accordingly includes a diurnal cycle for the PBL height. These amendments are discussed further in Sect. 2.4.
- Simulations start at 06:00 using spring equinoctical conditions and the simulations ended after two days.
- All simulations performed using the Master Chemical Mechanism, MCM v3.2, (Rickard et al., 2015), Common Representative Intermediates, CRI v2 (Jenkin et al., 2008), Model for Ozone and related chemical tracers, MOZART-4 (Emmons et al., 2010), Regional Acid Deposition Model, RADM2 (Stockwell et al., 1990) and the Carbon Bond Mechanism, CB05 (Yarwood et al., 2005). Coates and Butler (2015) describes the implementation of these chemical mechanisms for use with KPP within MECCA. These chemical mechanisms were chosen as they are commonly used by modelling groups and represent the highly-detailed chemistry (MCM v3.2), chemistry suitable for regional 3D models (CRI v2, RADM2 and CB05) and global 3D models (MOZART-4).
- NO<sub>x</sub> emissions and temperature were varied systematically to analyse the effects on ozone mixing ratios over different NO<sub>x</sub> gradients at each temperature.
- VOC emissions constant until noon of first day, to simulate a plume of emitted VOC.
- Two sets of runs were performed – to include both a temperature-dependent and temperature-independent source of biogenic VOC emissions. MEGANv2.1 (Guenther et al., 2012) was used to specify the temperature-dependent BVOC emissions of isoprene. Isoprene is the most important VOC at a global scale due its high emission rates and emissions from vegetation have been reported to depend on temperature (Guenther et al.,

2006). In reality, increased temperature can also increase AVOC emissions by increasing evaporation of NMVOCs, this is not included in our study.

- Methane is fixed at 1.7 ppmv throughout the model run, carbon monoxide (CO) and ozone were initialised at 200 ppbv and 40 ppbv and then allowed to evolve freely throughout the the simulation.
- The temperature was systematically varied between 288 and 313 K (15 – 40 °C). The only source of NOx emissions in the box model was a constant source of NO emissions. The NO emissions were systematically varied from  $5.0 \times 10^9$  to  $1.5 \times 10^{12}$  molecules (NO)  $\text{cm}^{-2} \text{s}^{-1}$  at each temperature used in this study.

## 2.2 VOC Emissions

- Anthropogenic emissions from Benelux for the year 2011 were obtained from the TNO-MACC\_III emission inventory. TNO-MACC\_III is the current version of the TNO-MACC\_II inventory and was created using the same methodology as Kuenen et al. (2014) and based upon improvements to the existing emission inventory during the AQMEII-2 exercises described in Pouliot et al. (2015).
- Temperature-independent emissions of the biogenic VOC isoprene and monoterpenes, were calculated as a fraction of the total anthropogenic VOC emissions from each country in the Benelux region, this data was obtained from the supplementary data available from the EMEP (European Monitoring and Evaluation Programme) model (Simpson et al., 2012).
- AVOC and BVOC emissions are included as total emissions from SNAP (Selected Nomenclature for Air Pollution) source categories and these emissions were assigned to chemical groupings based on the country specific profiles for Belgium, the Netherlands and Luxembourg provided by TNO.
- The MCM v3.2 initial species were determined using the country specific profiles for each SNAP source category and where appropriate information of individual chemical species that can be represented by MCM v3.2 were determined using the detailed speciations of Passant (2002). This approach was also used in von Schneidemesser et al. (2015) and further details are found within this article.

Table 1: Total anthropogenic NMVOC emissions in 2011 in tonnes from each SNAP category assigned from TNO-MACC\_III emission inventory and biogenic VOC emission in tonnes from Benelux region assigned from EMEP. The allocation of these emissions to MCM v3.2, CRI v2, CB05, MOZART-4 and RADM2 species is found in the supplement.

	<b>SNAP1</b>	<b>SNAP2</b>	<b>SNAP34</b>	<b>SNAP5</b>	<b>SNAP6</b>	<b>SNAP71</b>
Belgium	4494	9034	22152	5448	42809	6592
Netherlands	9140	12173	29177	8723	53535	16589
Luxembourg	121	44	208	1371	4482	1740
Total	13755	21251	62648	15542	100826	24921
	<b>SNAP72</b>	<b>SNAP73</b>	<b>SNAP74</b>	<b>SNAP8</b>	<b>SNAP9</b>	<b>BVOC</b>
Belgium	2446	144	210	6448	821	7042
Netherlands	3230	1283	1793	10067	521	1462
Luxembourg	1051	6	324	643	0	2198
Total	6727	1433	2327	17158	1342	10702

- As in von Schneidemesser et al. (2015), first the primary VOC that are represented by the MCM v3.2 and respective emissions were determined. Using this MCM v3.2 data, the NMVOC emission data were mapped to mechanism species in the other four chemical mechanisms used in the study. The NMVOC emissions in the non-MCM v3.2 chemical mechanisms were weighted by the carbon numbers of the MCM v3.2 species and the emitted mechanism species. The supplementary data outlines the primary NMVOC and calculated emissions with each chemical mechanism.

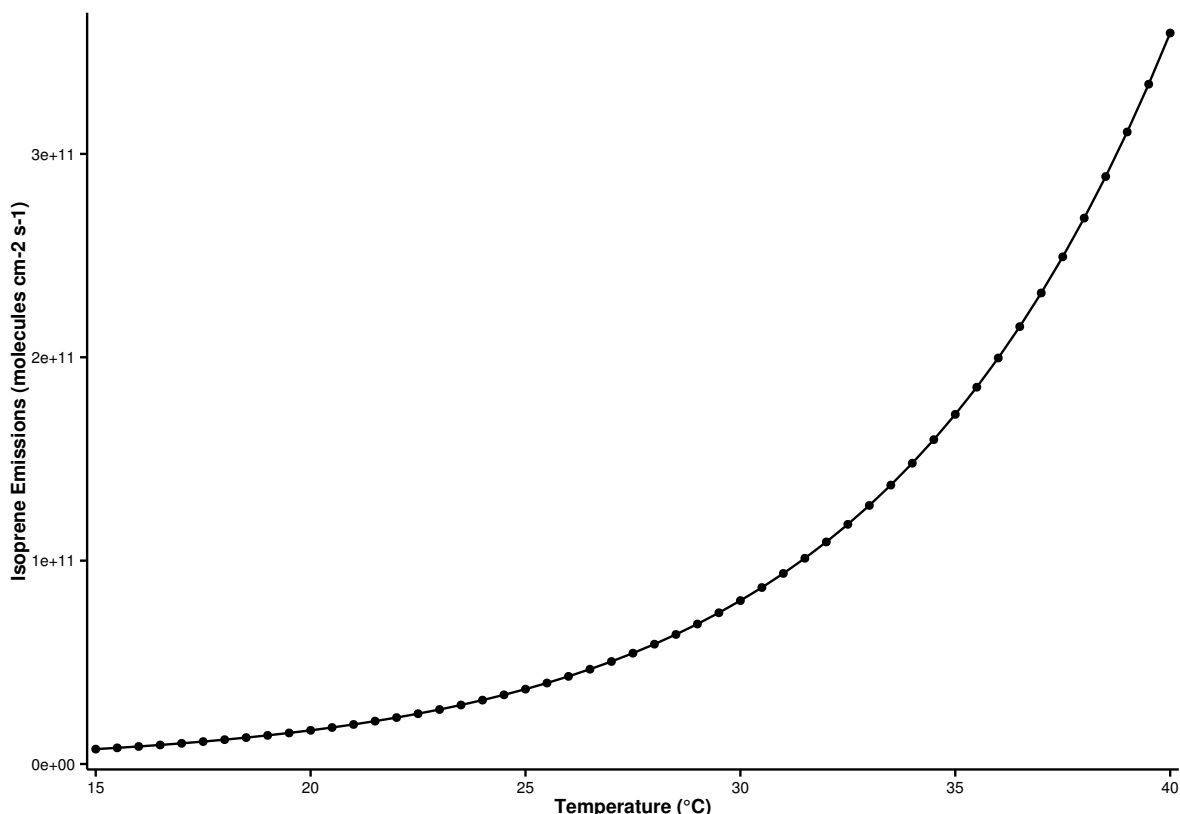
## 2.3 Temperature Dependent Isoprene Emissions

- Temperature dependent isoprene emissions were estimated using the MEGAN2.1 algorithm (Guenther et al., 2012).
- The aim of the study is to look at the effects of temperature, hence in the MEGAN2.1 algorithm all parameters (except temperature) were kept constant.
- The boxmodel setup uses a constant temperature throughout the model run and so the parameters  $T_{24}$  and  $T_{240}$ , the average temperatures in the past 24 and 250 hours, were assumed to be constant and equal to the temperature value of the boxmodel.
- Constant PAR (photosynthetically active radiation) and LAI (leaf area index) were used at each temperature step.
- The LAI, plant functional type (PFT) and associated isoprene emission factor were taken from Guenther et al. (2012) and selected to give the same isoprene mixing ratios at a temperature of 293 K as in the temperature independent modelling case. For all other model runs over the different temperature, the MEGAN2.1 algorithm was used to estimate the isoprene emissions.
- Thus using this idealised case, we can determine the effects of increasing isoprene emissions with temperature across  $\text{NO}_x$  gradients.
- This was repeated for each chemical mechanism.
- As in the temperature independent model runs, the emissions of NMVOC and the temperature dependent source of isoprene, were held constant until noon of the first day.
- Using these assumptions, the isoprene emissions at each temperature step of the study are illustrated in Fig. 1 and show the expected exponential increase in emissions with temperature (Guenther et al., 2006).

## 2.4 Vertical Mixing with Diurnal Boundary Layer Height

- The MECCA box model used in Coates and Butler (2015) included a constant boundary layer height of 1 km and no interactions (vertical mixing) with the free troposphere.

Figure 1: The estimated isoprene emissions (molecules isoprene  $\text{cm}^{-2} \text{s}^{-1}$ ) at each temperature step used in the study. Isoprene emissions were estimated using the MEGAN2.1 algorithm (Guenther et al., 2012).



- The planetary boundary layer (PBL) height varies diurnally and affects chemistry by diluting emissions after sunrise when the PBL rises. The expansion of the PBL into the free troposphere introduces vertical mixing with those chemical species present in the free troposphere. When the PBL collapses in the evening, pollutants are trapped in the PBL.
- The mixing layer height was measured as part of the BAERLIN campaign over the city of Berlin, Germany. The profile of mean mixing layer height during the campaign period (June – August 2014) was used in the model to represent the diurnal cycle of the mixing layer height.
- The concentrations of the chemical species within the PBL are diluted due to the larger mixing volume when the PBL height increases at the beginning of the day, also the increasing PBL height mixes the chemical species from the free troposphere with the chemical species within the PBL i.e. vertical mixing. The PBL height collapses during night leaving the stable nocturnal boundary layer, trapping the chemical species into a smaller volume thus increasing the concentrations of the chemical species.

Reference  
Boris'  
paper

Table 2: Increase in ozone mixing ratio (ppbv) due to chemistry and emissions at 40 °C from reference temperature (20 °C) in the NO<sub>x</sub>-regimes of Fig. 2.

Chemical Mechanism	Source of Difference	Increase in Ozone at 40 °C from 20 °C (ppbv)		
		Low-NO <sub>x</sub>	Maximal-O <sub>3</sub>	High-NO <sub>x</sub>
MCMv3.2	Chemistry	6.8	12.5	15.2
	Emissions	4.6	7.7	10.6
CRIV2	Chemistry	6.0	11.1	13.7
	Emissions	4.8	7.9	10.8
MOZART-4	Chemistry	6.0	10.2	12.3
	Emissions	4.1	6.7	10.0
CB05	Chemistry	9.3	16.0	19.9
	Emissions	4.6	7.4	9.8
RADM2	Chemistry	8.6	14.1	17.3
	Emissions	3.8	5.7	7.8

- This vertical mixing scheme was implemented into the boxmodel using the same approach of Lourens (2012).
- The mixing ratios of O<sub>3</sub>, CO and CH<sub>4</sub> in the free troposphere were respectively set to 50 ppbv, 116 ppbv and 1.8 ppmv. These conditions were taken from the MATCH-MPIC chemical weather forecast model on the 21st March (the start date of the simulations). The model results (<http://cwf.iass-potsdam.de/>) at the 700 hPa height were chosen and the daily average was used as input into the boxmodel.

check  
reference

### 3 Results and Discussion

#### 3.1 Ozone mixing ratios as function of NO<sub>x</sub> and Temperature

Figure 2 depicts the maximum mixing ratio of ozone as a function of the total NO<sub>x</sub> emissions on the first day and temperature when using temperature-independent and temperature-dependent source of isoprene emissions for each chemical mechanism. A non-linear relationship of ozone mixing ratios with NO<sub>x</sub> and temperature is reproduced by each chemical mechanism. This non-linear relationship has a similar form to that determined by Pusede et al. (2014) using an analytical model constrained to observational measurements over the San Joaquin Valley in California.

The highest mixing ratios of ozone in Fig. 2 are produced at higher temperatures and high-NO<sub>x</sub> conditions, also ozone mixing ratios increase when using a temperature-dependent source of isoprene emissions. Conversely, the least amount of ozone is produced with low-NO<sub>x</sub> conditions over the whole temperature range (15 – 40 °C) when using both a temperature-independent and



Figure 2: Contours of maximum ozone mixing ratio as a function of the total  $\text{NO}_x$  emissions on the first day and temperature for each chemical mechanism and using both a temperature-dependent and -independent source of isoprene emissions.

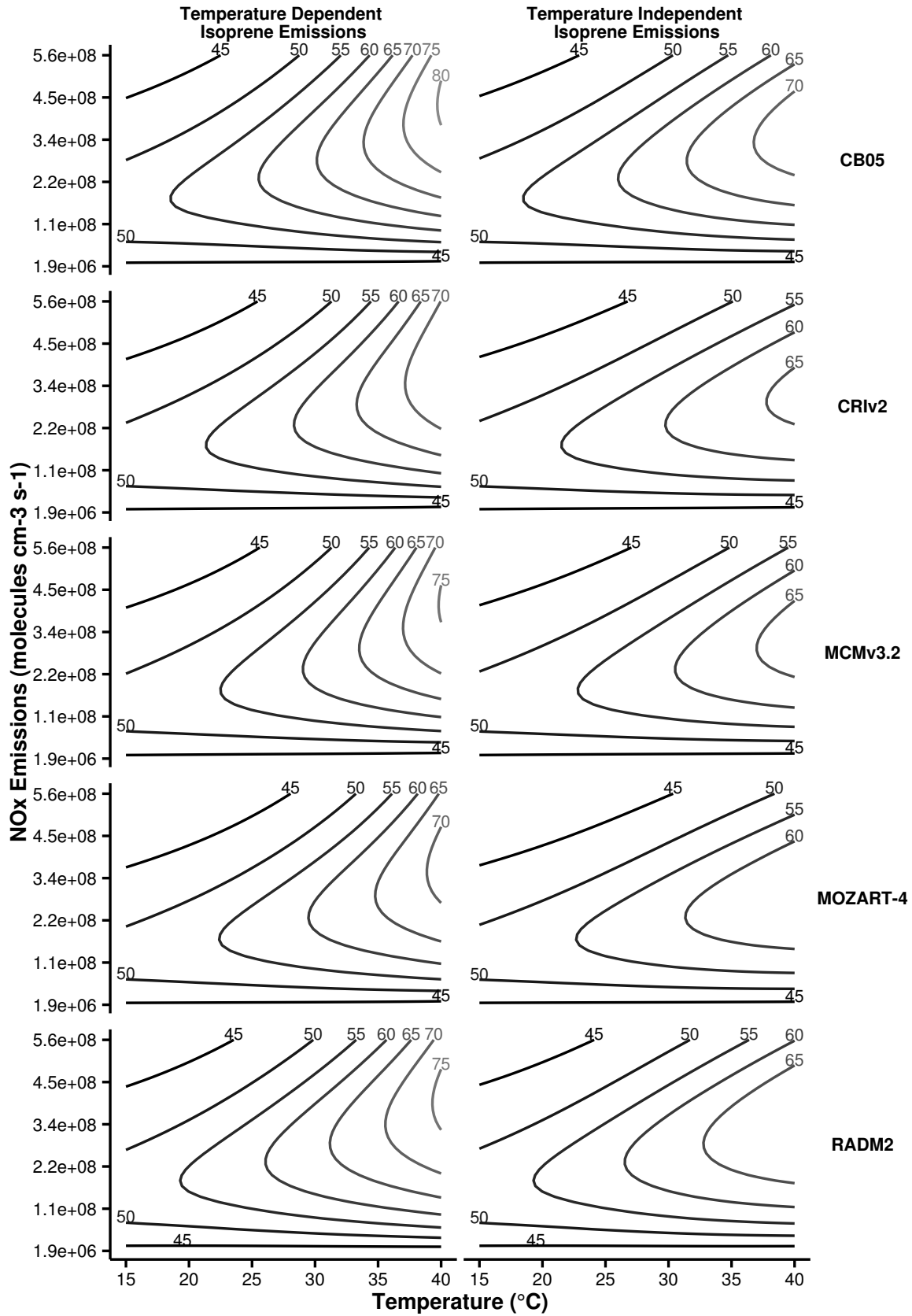
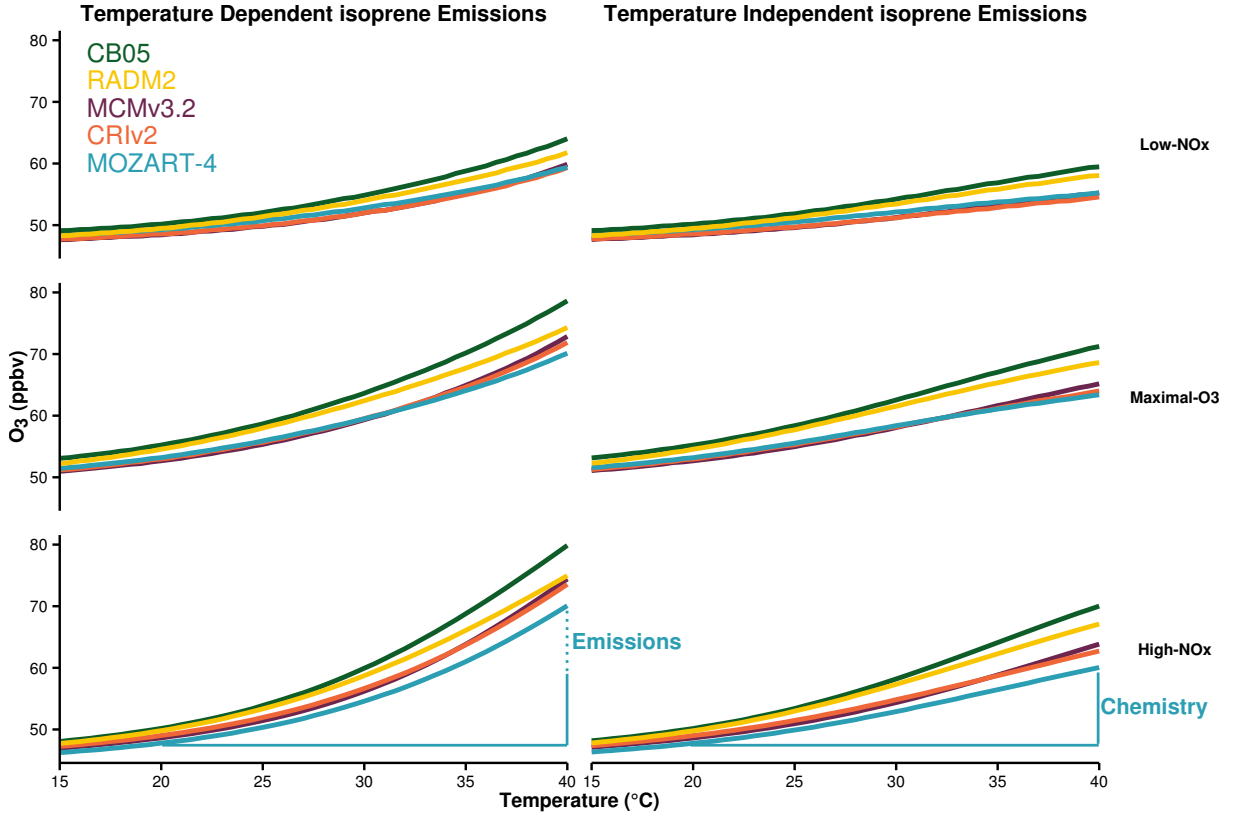


Figure 3: Ozone mixing ratios at each temperature are allocated to different  $\text{NO}_x$ -regimes of Fig. 2. The differences in ozone mixing ratios due to chemistry and emissions of Table 2 are represented graphically for MOZART-4, the approach was used to calculate the differences with each chemical mechanism.



temperature-dependent source of isoprene emissions.

The non-linear relationship of ozone with  $\text{NO}_x$  and temperature can be split into three  $\text{NO}_x$ -regimes (low- $\text{NO}_x$ , maximal- $\text{O}_3$  and high- $\text{NO}_x$ ) based on the ratio of  $\text{HNO}_3$  to  $\text{H}_2\text{O}_2$  used in Sillman (1995) to determine  $\text{NO}_x$ -regimes for the non-linear relationship of ozone with  $\text{NO}_x$  and VOC. The low- $\text{NO}_x$  regime corresponds to the lower-left most area in Fig. 2 where there is little increase in ozone with temperature, also called  $\text{NO}_x$ -sensitive conditions. The high- $\text{NO}_x$  regime is when ozone levels increase rapidly with temperature in Fig. 2, sometimes called  $\text{NO}_x$ -saturated conditions. Finally, the ridges of the contours in Fig. 2 correspond to maximal-ozone production and we call this the maximal- $\text{O}_3$  regime. The ozone mixing ratios obtained in each simulation were assigned to a  $\text{NO}_x$  regime based on the  $\text{H}_2\text{O}_2:\text{HNO}_3$  of the simulation and Fig. 3 illustrates the mean ozone mixing ratio at each temperature in these  $\text{NO}_x$  regimes.

Calculating the difference in ozone mixing ratios at 40 °C from 20 °C when using a temperature-independent source of isoprene emissions gives the absolute increase in ozone due to faster chemistry. When using a temperature-dependent source of isoprene emissions, the difference in ozone mixing ratios at 40 °C from 20 °C less the increase due to faster chemistry,

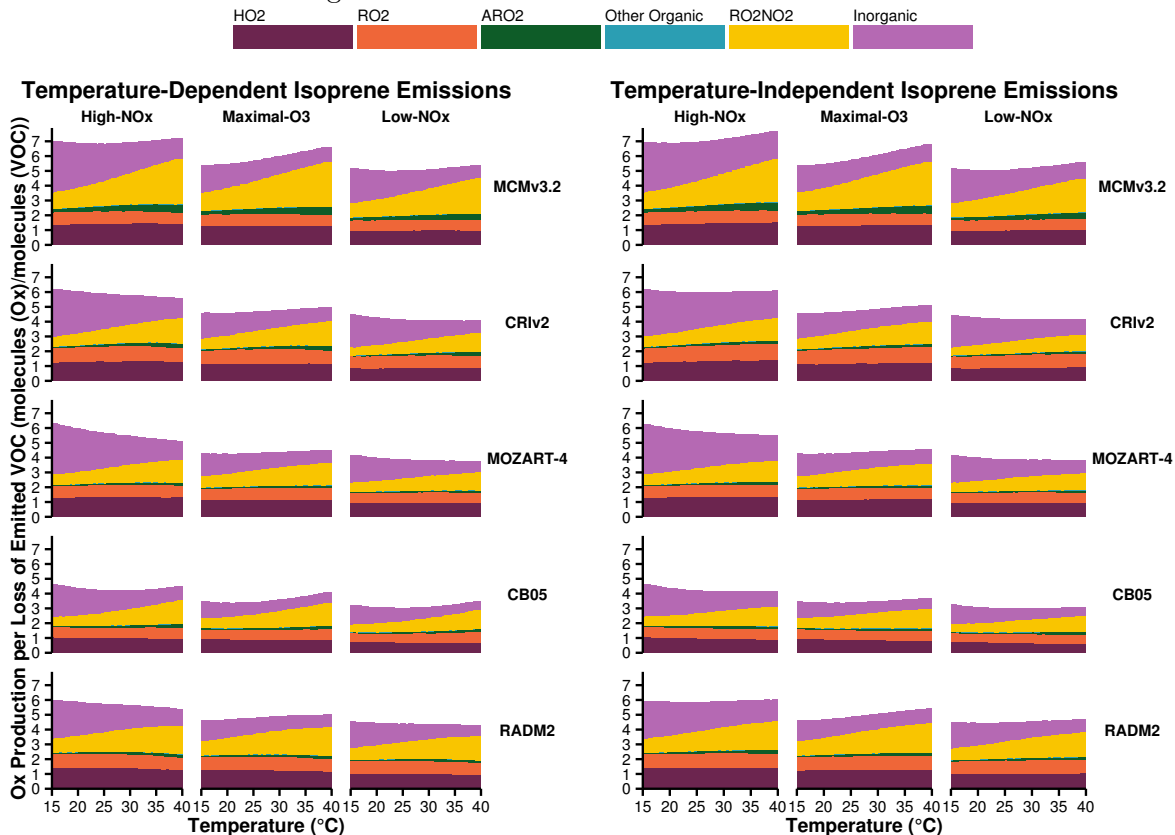
gives the absolute increase in ozone due to increased isoprene emissions. These differences are represented graphically in Fig. 3 and summarised in Table 2.

Both Fig. 3 and Table 2 highlight that the absolute increase in ozone at 40 °C from 20 °C is largest with high-NO<sub>x</sub> conditions. The increase in ozone mixing ratio at 40 °C from 20 °C due to faster chemistry with high-NO<sub>x</sub> conditions is almost double that with low-NO<sub>x</sub> conditions. We shall explore which chemical processes are responsible for the increases in ozone mixing ratios at 40 °C from 20 °C by analysing O<sub>x</sub> production budgets in Sect. 3.2.

Comparing the response of ozone mixing ratios to temperature in the reduced chemical mechanisms (CRIV2, MOZART-4, CB05 and RADM2) to the near-explicit MCMv3.2 chemical mechanism shows that the largest differences from the MCMv3.2 occur in the maximal-O<sub>3</sub> and high-NO<sub>x</sub> regimes. Table 2 also indicates that all reduced chemical mechanisms, except RADM2, have similar increases in ozone due to temperature-dependent isoprene emissions to MCMv3.2. RADM2 produces 3 ppbv less ozone than the MCMv3.2 due to temperature-dependent isoprene emissions consistently in each NO<sub>x</sub> regime, indicating that this difference is due to how isoprene degradation chemistry is treated in RADM2.

The Tagged Ozone Production Potential (TOPP) of isoprene is a measure of the number of molecules of ozone produced per molecule of isoprene emitted and Coates and Butler (2015) shows that less ozone is produced from isoprene degradation using RADM2 than with MCMv3.2. The degradation of isoprene has been extensively studied and it is well-known that the species methyl vinyl ketone (MVK) and methacrolein are signatures of isoprene degradation. All chemical mechanisms used in our study do explicitly include MVK and methacrolein (or in the case of CB05, a lumped species representing both these secondary degradation products) production during isoprene degradation except RADM2. RADM2 does not include methacrolein and the ketone species included in RADM2 represents a mixture of acetone and methyl ethyl ketone (MEK), thus the secondary degradation of isoprene in RADM2 is unable to represent the ozone production from the further degradation of its signature degradation products MVK and methacrolein. More recent versions of RADM2, RACM (Stockwell et al., 1997) and RACM2 (Goliff et al., 2013), sequentially include methacrolein and MVK and with these updates the TOPP values of isoprene reported in Coates and Butler (2015) are similar to the TOPP value of isoprene in the MCMv3.2.

Figure 4: Day-time  $O_x$  production budgets normalised by the total oxidation rate of emitted VOC in the  $NO_x$ -regimes of Fig. 2. The budgets are allocated to the categories of inorganic reactions, peroxy nitrate ( $RO_2NO_2$ ) decomposition, reactions of NO with  $HO_2$ , alkyl peroxy radicals ( $RO_2$ ) and acyl peroxy radicals ( $ARO_2$ ). All other reactions contributing to  $O_x$  budgets are allocated to ‘Other Organic’.



### 3.2 Ozone Production Budgets

In order to determine which chemical processes are causing the increase in ozone with temperature (Sect. 3.1), we analyse the  $O_x$  production budgets in each  $NO_x$  regime (low- $NO_x$ , Maximal- $O_3$  and high- $NO_x$ ) defined in Sect. 3.1. We defined the  $O_x$  family to consist of  $O_3$ ,  $NO_2$  and  $O$ , and Fig. 4 displays the total day-time  $O_x$  production budgets normalised by the total initial oxidation rates of the emitted NMVOC for each chemical mechanism within each  $NO_x$  regime. The  $O_x$  production budgets in Fig. 4 are allocated to the major sources, where ‘ $HO_2$ ’, ‘ $RO_2$ ’, ‘ $ARO_2$ ’ represent the reactions of NO with  $HO_2$ , alkyl peroxy radicals and acyl peroxy radicals respectively. ‘ $RO_2NO_2$ ’ represents the thermal decomposition of peroxy nitrates, ‘Inorganic’ represents all inorganic contributions to the  $O_x$  production budgets (primarily the de-excitation of  $O^1D$  to  $O$ ) and any other remaining organic reactions producing  $O_x$  are included in the ‘Other Organic’ category.

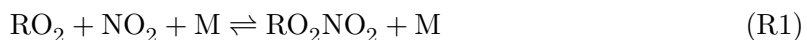
In Fig. 4 the number of molecules of  $O_x$  produced per molecule of NMVOC oxidised in

High-NO<sub>x</sub> conditions is similar when using temperature-dependent or temperature-independent isoprene emissions for each chemical mechanism; the same is also true for the Maximal-O<sub>3</sub> and Low-NO<sub>x</sub> regimes. Thus the increases in isoprene emissions in the temperature-dependent simulations are balanced by the faster oxidation rates of the emitted NMVOC. The highest amount of O<sub>x</sub> is produced in the High-NO<sub>x</sub> regime and the lowest amount of O<sub>x</sub> is produced in the Low-NO<sub>x</sub> regime, mirroring the O<sub>3</sub> mixing ratios in the different NO<sub>x</sub> regimes in Fig.3. For example, when using MCMv3.2 seven molecules of O<sub>x</sub> are produced per molecule of NMVOC oxidation in High-NO<sub>x</sub> conditions, decreased to about six and five molecules of O<sub>x</sub> produced per molecule of NMVOC oxidised in the Maximal-O<sub>3</sub> and Low-NO<sub>x</sub> regimes. In each NO<sub>x</sub> regime, all the reduced chemical mechanisms produce up to two molecules of O<sub>x</sub> per molecule of emitted NMVOC oxidised less than the MCMv3.2.

Turning to the individual contributions to the normalised production of O<sub>x</sub> in Fig. 4, peroxy nitrate (RO<sub>2</sub>NO<sub>2</sub>) decomposition and inorganic reactions show a strong (and opposing) dependence on temperature in all NO<sub>x</sub> regimes, each chemical mechanism and regardless of the source of isoprene emissions. Whereas the contributions of the reaction of NO with the peroxy radicals (HO<sub>2</sub>, RO<sub>2</sub> and ARO<sub>2</sub> in Fig. 4) to the normalised production budgets of O<sub>x</sub> do not increase strongly with temperature indicating that these processes are strongly related to the faster oxidation of the emitted NMVOC with temperature.

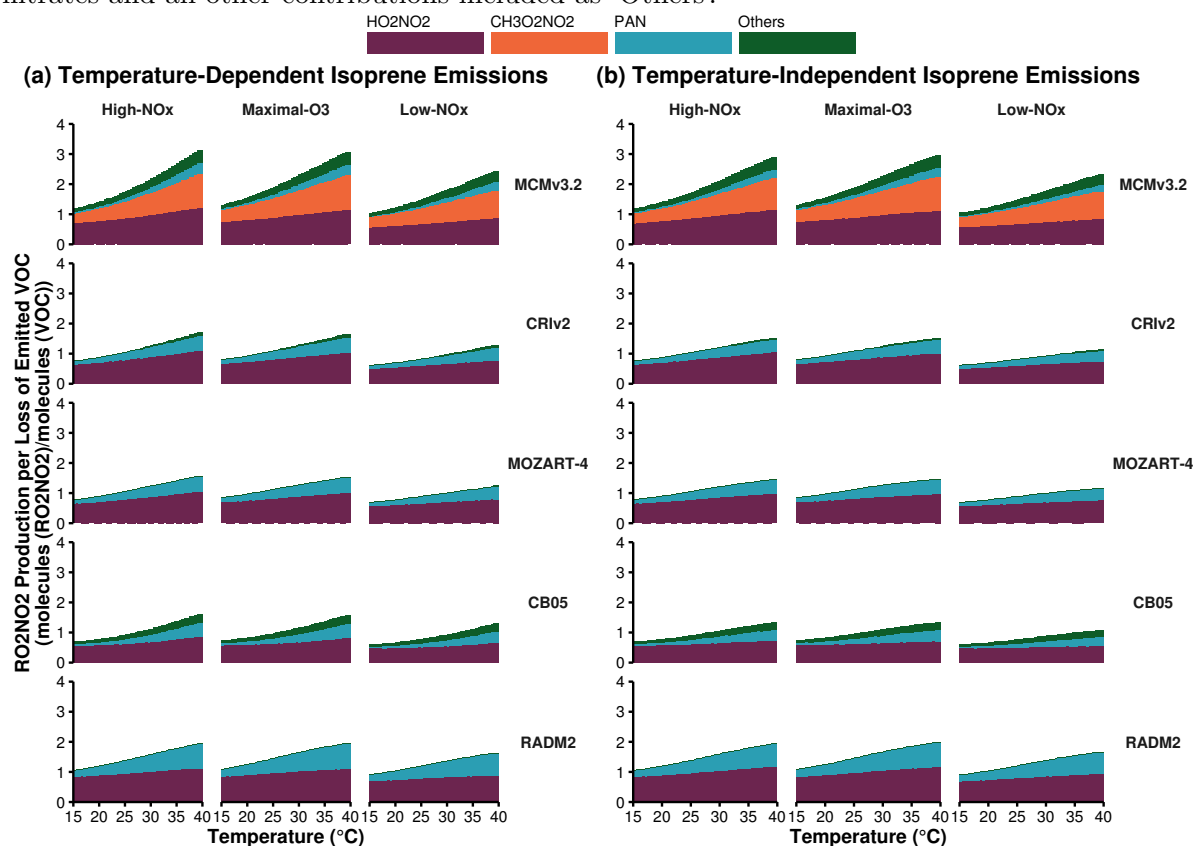
### 3.2.1 Peroxynitrates

We shall now turn our focus to the peroxy nitrate (RO<sub>2</sub>NO<sub>2</sub>) contribution as this category has a strongly temperature-dependent contribution to the normalised O<sub>x</sub> production. Peroxy nitrates are an important reservoir species for both peroxy radicals and NO<sub>x</sub> that are formed from the reactions of alkyl and acyl peroxy nitrates with NO<sub>2</sub> (Reaction R1).



The chemical bond of RO<sub>2</sub>NO<sub>2</sub> is quite weak with thermal decomposition being the most important chemical reaction and thermal decomposition depends strongly on temperature. At low temperatures, RO<sub>2</sub>NO<sub>2</sub> can accumulate and be transported downwind of emissions of the sources of its precursors (NMVOC and NO<sub>x</sub>), after thermal decomposition the release of NO<sub>2</sub> and peroxy radicals can promote production of O<sub>3</sub> downwind (Moxim et al., 1996).

Figure 5: Day-time  $\text{RO}_2\text{NO}_2$  production budgets normalised by the total oxidation rate of emitted VOC in the  $\text{NO}_x$ -regimes of Fig. 2. The total budgets are allocated to the most important peroxy nitrates and all other contributions included as ‘Others’.



Peroxy nitrates are formed from both alkyl and acyl peroxy radicals, with the acyl peroxy radicals being more thermally stable than the alkyl peroxy nitrates. The most important alkyl peroxy nitrates are pernitric acid ( $\text{HO}_2\text{NO}_2$ ) and methylperoxy nitrate ( $\text{CH}_3\text{O}_2\text{NO}_2$ ), while peroxy acetyl nitrate (PAN,  $\text{CH}_3\text{C}(\text{O})\text{O}_2\text{NO}_2$ ) and peroxy propionyl nitrate (PPN,  $\text{C}_2\text{H}_5\text{C}(\text{O})\text{O}_2\text{NO}_2$ ) are important acyl peroxy nitrates.

The alkyl peroxy nitrates have a weaker  $\text{RO}_2\text{—NO}_2$  bond than acyl peroxy nitrates hence alkyl peroxy nitrates have a shorter lifetime than acyl peroxy nitrates. For example,  $\text{CH}_3\text{O}_2\text{NO}_2$  has a lifetime of 0.5 seconds at 298 K while PAN has a lifetime of 51 minutes at 298 K (Orlando and Tyndall, 2012).

Each chemical mechanism used in our study represents  $\text{HO}_2\text{NO}_2$  and PAN, although in many reduced chemical mechanisms PAN represents  $\text{CH}_3\text{C}(\text{O})\text{O}_2\text{NO}_2$  and other acyl peroxy nitrates. This representation of PAN in reduced chemical mechanisms can lead to overestimations of PAN levels compared to more detailed chemical mechanisms (Luecken et al., 1999). The near-explicit MCMv3.2 represent a diverse range of peroxy nitrates including  $\text{CH}_3\text{O}_2\text{NO}_2$  and about 280 acyl peroxy nitrates.

Figure 5 displays the normalised production budgets of  $\text{RO}_2\text{NO}_2$  by the total loss rate of the emitted NMVOC, similar to Fig. 4 for each chemical mechanism in each  $\text{NO}_x$  regime and when using a temperature-independent and temperature-dependent source of isoprene emissions. The large contribution of  $\text{CH}_3\text{O}_2\text{NO}_2$  in MCMv3.2 is not mirrored in any reduced chemical mechanism as  $\text{CH}_3\text{O}_2\text{NO}_2$  is not represented in any of the reduced chemical mechanisms. In fact the number of molecules of  $\text{RO}_2\text{NO}_2$  per molecules of NMVOC oxidised in each reduced chemical mechanism is very similar to that of MCMv3.2 less the contribution of  $\text{CH}_3\text{O}_2\text{NO}_2$  for the separate  $\text{NO}_x$  regimes and regardless of isoprene source.

The contribution of  $\text{RO}_2\text{NO}_2$  to the normalised  $\text{O}_x$  production in Fig. 4 is largest in the MCMv3.2 than the reduced chemical mechanisms due to the representation of  $\text{CH}_3\text{O}_2\text{NO}_2$  in the MCMv3.2. If reduced chemical mechanisms represent  $\text{CH}_3\text{O}_2\text{NO}_2$  chemistry then this would improve the representation of the total  $\text{RO}_2\text{NO}_2$  production which would have the added effect of improving the representation of  $\text{O}_x$  production budgets.

## 4 Conclusions

## References

- William P. L. Carter, Arthur M. Winer, Karen R. Darnall, and James N. Pitts Jr. Smog chamber studies of temperature effects in photochemical smog. *Environmental Science & Technology*, 13(9):1094–1100, 1979.
- J. Coates and T. M. Butler. A comparison of chemical mechanisms using tagged ozone production potential (TOPP) analysis. *Atmospheric Chemistry and Physics*, 15(15):8795–8808, 2015.
- John P. Dawson, Peter J. Adams, and Spyros N. Pandis. Sensitivity of ozone to summertime climate in the eastern USA: A modeling case study . *Atmospheric Environment*, 41(7):1494 – 1511, 2007.
- L. K. Emmons, S. Walters, P. G. Hess, J.-F. Lamarque, G. G. Pfister, D. Fillmore, C. Granier, A. Guenther, D. Kinnison, T. Laepple, J. Orlando, X. Tie, G. Tyndall, C. Wiedinmyer, S. L. Baughcum, and S. Kloster. Description and evaluation of the Model for Ozone and Related chemical Tracers, version 4 (MOZART-4). *Geoscientific Model Development*, 3(1):43–67, 2010.

307 Wendy S. Goliff, William R. Stockwell, and Charlene V. Lawson. The regional atmospheric  
 308 chemistry mechanism, version 2. *Atmospheric Environment*, 68:174 – 185, 2013.

309 A. Guenther, T. Karl, P. Harley, C. Wiedinmyer, P. I. Palmer, and C. Geron. Estimates of global  
 310 terrestrial isoprene emissions using MEGAN (Model of Emissions of Gases and Aerosols from  
 311 Nature). *Atmospheric Chemistry and Physics*, 6(11):3181–3210, 2006.

312 A. B. Guenther, X. Jiang, C. L. Heald, T. Sakulyanontvittaya, T. Duhl, L. K. Emmons, and  
 313 X. Wang. The Model of Emissions of Gases and Aerosols from Nature version 2.1 (MEGAN2.1):  
 314 an extended and updated framework for modeling biogenic emissions. *Geoscientific Model  
 315 Development*, 5(6):1471–1492, 2012.

316 Shiro Hatakeyama, Hajime Akimoto, and Nobuaki Washida. Effect of temperature on the  
 317 formation of photochemical ozone in a propene-nitrogen oxide (NO<sub>x</sub>)-air-irradiation system.  
 318 *Environmental Science & Technology*, 25(11):1884–1890, 1991.

319 Daniel J. Jacob and Darrell A. Winner. Effect of climate change on air quality. *Atmospheric  
 320 Environment*, 43(1):51 – 63, 2009. Atmospheric Environment - Fifty Years of Endeavour.

321 M.E. Jenkin, L.A. Watson, S.R. Utembe, and D.E. Shallcross. A Common Representative  
 322 Intermediates (CRI) mechanism for VOC degradation. Part 1: Gas phase mechanism development.  
 323 *Atmospheric Environment*, 42(31):7185 – 7195, 2008.

324 J. J. P. Kuenen, A. J. H. Visschedijk, M. Jozwicka, and H. A. C. Denier van der Gon.  
 325 TNO-MACC\_II emission inventory; a multi-year (2003–2009) consistent high-resolution european  
 326 emission inventory for air quality modelling. *Atmospheric Chemistry and Physics*, 14(20):  
 327 10963–10976, 2014.

328 AsM Lourens. *Air quality in the Johannesburg-Pretoria megacity: its regional influence and  
 329 identification of parameters that could mitigate pollution*. PhD thesis, North-West University,  
 330 Potchefstroom Campus, 2012.

331 D.J. Luecken, G.S. Tonnesen, J.E. Sickles, and II. Differences in noy speciation predicted by  
 332 three photochemical mechanisms. *Atmospheric Environment*, 33(7):1073 – 1084, 1999.

333 W. J. Moxim, H. Levy, and P. S. Kasibhatla. Simulated global tropospheric PAN: Its transport  
 334 and impact on NO<sub>x</sub>. *Journal of Geophysical Research: Atmospheres*, 101(D7):12621–12638, 1996.



John J. Orlando and Geoffrey S. Tyndall. Laboratory studies of organic peroxy radical chemistry: an overview with emphasis on recent issues of atmospheric significance. *Chem. Soc. Rev.*, 41: 6294–6317, 2012.

N. Passant. Speciation of UK emissions of non-methane volatile organic compounds. Technical report, DEFRA, Oxon, UK., 2002.

George Pouliot, Hugo A.C. Denier van der Gon, Jeroen Kuenen, Junhua Zhang, Michael D. Moran, and Paul A. Makar. Analysis of the emission inventories and model-ready emission datasets of Europe and North America for phase 2 of the AQMEII project. *Atmospheric Environment*, 115: 345–360, 2015.

S. E. Pusede, D. R. Gentner, P. J. Wooldridge, E. C. Browne, A. W. Rollins, K.-E. Min, A. R. Russell, J. Thomas, L. Zhang, W. H. Brune, S. B. Henry, J. P. DiGangi, F. N. Keutsch, S. A. Harrold, J. A. Thornton, M. R. Beaver, J. M. St. Clair, P. O. Wennberg, J. Sanders, X. Ren, T. C. VandenBoer, M. Z. Markovic, A. Guha, R. Weber, A. H. Goldstein, and R. C. Cohen. On the temperature dependence of organic reactivity, nitrogen oxides, ozone production, and the impact of emission controls in San Joaquin Valley, California. *Atmospheric Chemistry and Physics*, 14(7):3373–3395, 2014.

Sally E. Pusede, Allison L. Steiner, and Ronald C. Cohen. Temperature and Recent Trends in the Chemistry of Continental Surface Ozone. *Chemical Reviews*, 115(10):3898–3918, 2015.

D. J. Rasmussen, Jianlin Hu, Abdullah Mahmud, and Michael J. Kleeman. The ozone–climate penalty: Past, present, and future. *Environmental Science & Technology*, 47(24):14258–14266, 2013. PMID: 24187951.

Andrew Rickard, Jenny Young, M. J. Pilling, M. E. Jenkin, Stephen Pascoe, and S. M. Saunders. The Master Chemical Mechanism Version MCM v3.2. <http://mcm.leeds.ac.uk/MCMv3.2/>, 2015. [Online; accessed 25-March-2015].

Sanford Sillman. The use of NO<sub>y</sub>, H<sub>2</sub>O<sub>2</sub>, and HNO<sub>3</sub> as indicators for ozone-NO<sub>x</sub>-hydrocarbon sensitivity in urban locations. *Journal of Geophysical Research: Atmospheres*, 100(D7): 14175–14188, 1995.

Sanford Sillman. The relation between ozone, NO<sub>x</sub> and hydrocarbons in urban and polluted rural environments. *Atmospheric Environment*, 33(12):1821 – 1845, 1999.

364 Sanford Sillman and Perry J. Samson. Impact of temperature on oxidant photochemistry in  
 365 urban, polluted rural and remote environments. *Journal of Geophysical Research: Atmospheres*,  
 366 100(D6):11497–11508, 1995.

367 D. Simpson, A. Benedictow, H. Berge, R. Bergström, L. D. Emberson, H. Fagerli, C. R. Flechard,  
 368 G. D. Hayman, M. Gauss, J. E. Jonson, M. E. Jenkin, A. Nyíri, C. Richter, V. S. Semeena,  
 369 S. Tsyro, J.-P. Tuovinen, Á. Valdebenito, and P. Wind. The EMEP MSC-W chemical transport  
 370 model – technical description. *Atmospheric Chemistry and Physics*, 12(16):7825–7865, 2012.

371 William R. Stockwell, Paulette Middleton, Julius S. Chang, and Xiaoyan Tang. The second  
 372 generation regional acid deposition model chemical mechanism for regional air quality modeling.  
 373 *Journal of Geophysical Research: Atmospheres*, 95(D10):16343–16367, 1990.

374 William R. Stockwell, Frank Kirchner, Michael Kuhn, and Stephan Seefeld. A new mechanism  
 375 for regional atmospheric chemistry modeling. *Journal of Geophysical Research: Atmospheres*,  
 376 102(D22):25847–25879, 1997.

377 E. von Schneidemesser, J. Coates, A. J. H. Visschedijk, H. A. C. Denier van der Gon, and T. M.  
 378 Butler. Variation of the NMVOC speciation in the solvent sector and the sensitivity of modelled  
 379 tropospheric ozone. *Atmospheric Environment*, page In preparation, 2015.

380 Greg Yarwood, Sunja Rao, Mark Yocke, and Gary Z. Whitten. Updates to the Carbon Bond  
 381 Chemical Mechanism: CB05. Technical report, U. S Environmental Protection Agency, 2005.